ITC 3/55
Information Technology and Control
Vol. 55 / No. 3/ 2026
pp. 1100-1111
DOI 10.5755/j01.itc.55.3.44894

SR-CNN: Outlier Detection Preprocessing for Low-Dose CT Noise Equalization

Received 2026/04/29 | Accepted after revision 2026/06/30

HOW TO CITE: Zhou, B., Liang, Y., Zhang, Q. (2026) SR-CNN: Outlier Detection Preprocessing for Low-Dose CT Noise Equalization. *Information Technology and Control*, 55(3), 1098-1109. https://doi.org/10.5755/j01.itc.55.3.44894

SR-CNN: Outlier Detection Preprocessing for Low-Dose CT Noise Equalization

Bochao Zhou
School of Information and Communication Engineering, North University of China, Taiyuan, 030051, China; e-mail: 2671237388@qq.com

Yaxing Liang
Shaanxi Medical Products Administration, Xi'an, 710000, China; e-mail: 2107493369@qq.com

Quan Zhang*
School of Information and Communication Engineering, North University of China, Taiyuan, 030051, China; e-mail: zbc980218@163.com

Corresponding author: zbc980218@163.com

Low-dose computed tomography (LDCT) mitigates X-ray risks yet yields noisy images. Conventional unified denoising ignores spatially uneven noise, failing to suppress high-noise region interference and limiting performance. The core of this work is to equalize the spatially uneven noise distribution of LDCT images via a dedicated preprocessing strategy, so as to fully activate the denoising potential of mainstream algorithms. We first trained an outlier detection model to locate high-noise pixels in LDCT images. An image restoration model inspired by image inpainting was then developed to repair detected outliers, yielding LDCT images with spatially uniform noise. The preprocessed images were finally fed into conventional LDCT denoising algorithms for further processing. Evaluated on the public Mayo LDCT dataset, our preprocessing strategy increased the average PSNR by 1.5283 dB and SSIM by 0.8%, and reduced the RMSE by 4.911 HU when compared with raw LDCT images used as inputs for various denoising approaches. Thus, the Slide Region-based Convolutional Neural Network (SR-CNN) method provides a novel universal preprocessing approach for LDCT imaging by normalizing heterogeneous noise distribution, effectively enhancing image quality.

KEYWORDS: Low-dose computed tomography Image, Image denoising, Outlier detection, Deep learning

1. Introduction

As computed tomography (CT) imaging becomes increasingly prevalent in medical diagnostics, the potential harm of CT imaging on the human body has garnered widespread attention [22, 23]. Low-dose CT reduces radiation dose to minimize harm, but inevitably, this reduction leads to decreased image quality. A prominent and long-standing problem of LDCT images is the spatially uneven noise distribution caused by tube current, scanning position and slice thickness. Most existing denoising algorithms process LDCT images as a whole without targeted designs for heterogeneous noise. This leads to over-smoothing in low-noise regions and insufficient denoising in high-noise areas, which severely limits the performance of current denoising methods. Equalizing the spatial distribution of noise is the key to breaking this bottleneck, Solving the problem of uneven noise distribution is therefore of great significance for improving LDCT image quality. To improve the image quality of low-dose CT scans, two types of algorithms have been studied: traditional algorithms and deep learning algorithms. Traditional algorithms include K-Singular Value Decomposition (K-SVD) [21], nonlocal means (NLM) [36], and block-matching 3D (BM3D) [27]. Current deep learning algorithms primarily utilize Convolutional Neural Networks (CNNs) [15, 18, 34]. For example, Chen et al. introduced the deconvolution network and shortcut connections into the CNN model, proposing the RED-CNN (residual encoder-decoder convolutional neural network) [3]. Yuan et al. proposed a hybrid CNN-Transformer network model called HCformer, which effectively combines the local information processing capability of CNNs with the global computation capability of Transformers [32]. Han et al. developed a CNN model based on activation maps to preserve small image features [8]. However, CNN-based methods often result in over-smoothing of images [14, 20]. To address this issue, generative adversarial networks (GANs) have been introduced to preserve more image details [1, 4, 9, 29]. For instance, Huang et al. proposed a dual-domain U-Net based GAN network, which learns the differences between LDCT images and NDCT (normal dose CT) images in both the image domain and the gradient domain [10]. Yin et al. incorporated segmentation information into GAN networks to enhance the denoising effect by improving the accuracy of the segmentation model [31]. Chen et al. introduced the use of Cycle GANs to denoise LDCT images on unpaired datasets [12]. However, most LDCT methods treat the LDCT image as a whole during denoising, without designing specific modules to handle varying noise intensities. This leads to overly smooth denoising results in low-noise-intensity regions and insufficient denoising capability in high-noise-intensity areas.

Over recent years, transformer models [16, 33] and diffusion models [13, 6, 17, 24, 28] have garnered significant attention. Compared to CNN models, transformer models are more adept at capturing global information and long-range feature interactions, thereby utilizing more comprehensive information [2]. For instance, Zhang et al. first applied transformer models for LDCT denoising [35]. Wang et al. proposed the Convolution-free Token2Token Dilated Vision Transformer (CTformer) model, which entirely eliminates convolution operations, optimizing the performance of transformer models and developing interpretability for the CTformer with the visual attention maps and an explanatory graph [26]. Compared to GAN models, diffusion models can provide an analytical representation of data distribution during the generation process, enabling more advanced generation results [25, 30]. For example, Gao et al. proposed a contextual error-modulated generalized diffusion model (CoreDiff), which reduces accumulated errors and enhances model inference speed [7]. Liu et al. developed a fully unsupervised denoising model based on diffusion models, addressing the challenge of acquiring training data for LDCT image denoising [19]. Despite the significant success of the aforementioned methods in LDCT image denoising, they often treat LDCT images as a whole, overlooking the uneven noise intensity distribution caused by factors such as tube current, CT positioning, and slice thickness [11]. Moreover, most LDCT methods cannot differentiate between varying noise intensities for targeted denoising. We believe that addressing the uneven noise intensity distribution could further unlock the potential of existing LDCT denoising methods. The uneven noise of LDCT is manifested as scattered local high-noise

pixels/regions mixed in low-noise backgrounds. Such locally abnormal pixels conform to the typical characteristics of outliers in image data. Therefore, outlier detection technology is naturally suitable for locating these discrete high-noise points. Different from global denoising methods, outlier detection can accurately lock abnormal noise pixels without interfering with normal low-noise areas.

Different from the above strategies, our work does not redesign denoising network structures. Instead, we propose a dedicated preprocessing framework to adjust and unify the spatially uneven noise distribution of raw LDCT images. As a general plug-and-play preprocessing module, the proposed SR-CNN can be flexibly embedded into various existing LDCT denoising pipelines without modifying their original architectures, which greatly improves the applicability and scalability of the noise homogenization strategy.

In this paper, we propose an image preprocessing method based on outlier detection, featuring the three key characteristics. First, most existing methods do not account for the uneven noise intensity distribution in LDCT images. To identify and denoise different noise intensities, models often need to be redesigned. Therefore, we have designed a universal image preprocessing method to address the uneven noise intensity distribution in LDCT images, enhancing the denoising performance of existing methods without requiring model redesign. Second, to preserve image detail, we introduced structural similarity weights in the outlier detection process, preventing structural loss due to overly concentrated outliers. Third, to achieve a uniform noise intensity distribution in LDCT images and maintain the same input structure as existing methods, we incorporated an image restoration module. This module treats outliers as missing points and restores LDCT images to a uniform noise intensity distribution, aligning with the inputs of existing LDCT methods.

In summary, the contributions of this research are three-fold:

1 A general image preprocessing model based on outlier detection, SR-CNN, is proposed to address the shortcomings of existing LDCT methods that overlook the uneven noise intensity distribution in LDCT images. This is a standalone dedicated preprocessing model specially designed for LDCT noise homogenization. Unlike methods that embed adaptive noise processing branches into integrated end-to-end denoising networks, our module can be cascaded with existing denoising algorithms without modifying downstream network architectures and improves the denoising performance of downstream networks.

2 By integrating the detection model and the image restoration model, this method achieves uniform noise intensity distribution in LDCT images, enhancing the denoising performance of existing LDCT methods while preserving detailed information.

3 Tests performed on Mayo LDCT scans demonstrate that the integration of a preprocessing module enables multiple denoising techniques to yield noticeable improvements in both perceptual quality and quantitative metrics.

2. Methods

2.1. Dataset

We adopted the 2016 NIH-AAPM Mayo LDCT open-competition dataset, which comprises 2,378 paired low-dose and full-dose images with a slice thickness of 3 mm, derived from ten anonymized cases. Specifically, the data from patient L506 was designated as the independent evaluation set, whereas the remaining nine cases were fully utilized for network parameter optimization.

2.2. Abnormal Point

Existing literature has established that LDCT noise presents distinct spatial inhomogeneity [5]. To characterize this noise distribution, we leveraged the paired low- and full-dose image dataset from the 2016 NIH-AAPM Mayo LDCT Grand Challenge, and computed voxel-wise absolute differences between corresponding low-dose and full-dose images to construct noise distribution maps. Figure 1(a)-(d) presents the LDCT image and its local noise intensity distribution. Figure 1(d) shows the noise intensity distribution of the LDCT image, where the horizontal axis represents noise intensity, and the vertical axis represents the number of pixels corresponding to the noise intensity. The size of the LDCT image is 512 × 512. The results of

Figure 1(d) indicate that the noise intensity distribution in LDCT images is uneven. Specifically, there are significant variations in the noise intensity distribution, with a majority of pixels having low noise intensity and only a small portion of pixels exhibiting high noise intensity. However, most LDCT methods treat the LDCT image as a whole during denoising, without designing specific modules to handle varying noise intensities. This leads to overly smooth denoising results in low-noise-intensity regions and insufficient denoising capability in high-noise-intensity areas. To address these shortcomings, In this work, we define outliers as pixels with abnormally high noise intensity within their local neighborhoods. Different from normal pixels, these outlier pixels have noise levels significantly higher than surrounding pixels, and they are the main components causing uneven noise distribution in LDCT images. Based on this information, we designed the following method to detect outliers in LDCT images:

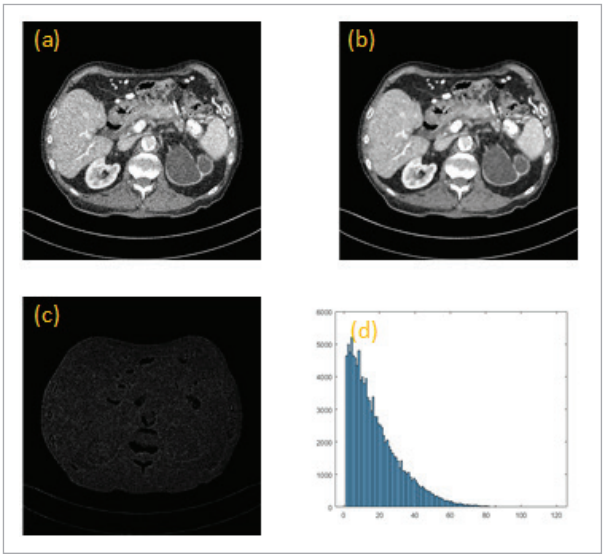
$$\theta_i = abs\left(f(i) - f_l(i)\right) * \left(1 - S_{w,w_l}\right) * \frac{1}{Z(w)} * d\left(||w - w_l||^2_{2,\beta}\right) \quad (1)$$

$$\alpha = h * mean(f - f_l) * \frac{1}{Z(f)} * d\left(||f - f_l||^2_{2,\beta}\right), \quad (2)$$

If $\theta_i > \alpha$, the point is considered an outlier. Here, f represents the NDCT image, and f_l represents the LDCT image; $f(i)$ and $f_l(i)$ are the points at the same location in the NDCT and LDCT images, respectively. The neighborhoods of these points are represented by w, w_l. The structural similarity value (SSIM) between neighborhoods w and f_l_l is denoted as S_{w,w_l}, and $Z(w)$ represents the number of elements in neighborhood w. The Gaussian-weighted Euclidean distance between neighborhoods w and w_l, used to calculate their similarity, is denoted as $d(||w–w_l||^2_{2,\beta})$. The parameter h controls the number of outliers, and $Z(f)$ represents the number of elements in f. The Gaussian-weighted Euclidean distance between f and f_l is denoted as $d(||f–f_l||^2_{2,\beta})$.To determine outliers based on noise intensity, the noise intensity at the same points in NDCT and LDCT images, $abs(f(i)–f_l(i))$, is first calculated. The mean noise intensity of the entire image, $mean(f–f_l)$, serves as a baseline.

Figure 1

Noise intensity distribution in LDCT Images. (a) LDCT image (b) NDCT image (c) Noise Intensity in an LDCT Image (d) Noise intensity distribution in an LDCT image (horizontal axis: noise intensity; vertical axis: number of pixels). Display window: [-160, 240] HU. This figure verifies that LDCT images present severely uneven noise distribution: most pixels have low noise intensity, while a small number of local pixels show extremely high noise.



To avoid losing detail, we aim for outliers to be distributed in regions where LDCT and NDCT images have significant structural differences. Therefore, S_{w,w_l} is used as a measure of structural difference, where a lower S_{w,w_l} value indicates greater structural difference. Using $(1–S_{w,w_l})$ assigns higher weights to points with significant structural differences. Finally, due to varying noise intensities across different regions of the LDCT image, the Gaussian-weighted Euclidean distance between the neighborhood of the point and the entire image is calculated as a weight to offset the noise intensity differences caused by different regions. The threshold $\theta_i > \alpha$ acts as the core criterion to distinguish normal pixels and high-noise outliers. f and f_l stand for reference NDCT images and target LDCT images respectively, while w, w_l denote local pixel neighborhoods for regional analysis. S_{w,w_l} quantifies local structural similarity and $Z(w)$ are applied for data normalization. The Gaussian-weighted Euclidean distance is adopted to measure regional and global image differences and compensate for regional noise deviations. Hyperparameter h is used to adjust the outlier detec-

tion sensitivity. The term $abs(f(i)-f_l(i))$ extracts real pixel-level noise, and $mean(f-f_l)$ works as the global noise baseline. The weight $(1-S_{w,w_l})$ prevents normal tissue details from being misjudged as noise. The distance-based weight eliminates the interference of uneven noise distribution.

Given that the uneven noise of LDCT is dominated by isolated high-noise pixels in local areas, we adopt outlier detection to separate these abnormal noise points from normal image pixels, which provides a feasible way to eliminate noise heterogeneity.

By calculating the pixel-wise difference between paired LDCT and NDCT images, we can accurately obtain the real noise intensity of each LDCT pixel and generate reliable ground-truth outlier labels for model training. The above label generation process based on paired LDCT-NDCT data is only performed in the offline training stage. After training is completed, the learned detection model can directly predict outliers by taking only single LDCT images as input in practical testing and clinical deployment. No NDCT images are required during the entire inference process. The model learns the implicit feature distribution of high-noise outliers from training data, so it can maintain stable detection performance for unseen LDCT data.

2.3. SR-CNN

As shown in Figure 2, the proposed SR-CNN adopts a two-step cascade model. The core objective of the entire framework is to equalize the uneven spatial noise of LDCT images, where the first model is a detection model designed to identify outliers in LDCT images. The second model is an image restoration model, which treats the detected outliers as missing points and restores the LDCT image to a uniform noise intensity distribution. This restoration ensures compatibility with existing LDCT methods without necessitating their redesign. To validate the performance of the SR-CNN network, we selected the NLM algorithm from traditional methods, the RED-CNN from CNN-based networks, the CTformer from transformer-based methods, and the Dn-Dp (Denoising with Diffusion Prior) from diffusion-based models. Each of these methods is a classic in its respective field and has achieved excellent results in low-dose CT image denoising.

2.3.1. Detection Model

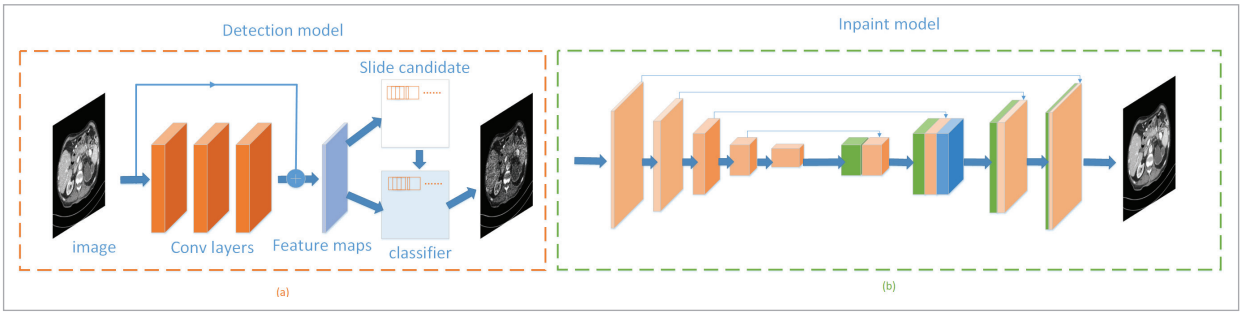
Due to the difficulty of matching LDCT images with NDCT images in real-world scenarios, we used LDCT images as an input and the outliers detected using the method described in Section 2.1 as an output. We trained a detection model to identify outliers even when only LDCT images are available. As shown in Figure 2(a), this model consists of three main components: convolutional layers, a sliding region generator, and a classifier.

2.3.1.1. The Convolutional Layer

The convolution layer extracts the feature map of the input image and employs a shallow network because the deeper convolutional layer has a larger receptive field. Since our aim was to detect the abnormal points by analyzing the neighborhood, we needed to ensure that the receptive field that was mapped to the image was not too large. Therefore, we employed a three-layer convolutional layer with convolution kernels of 1 × 1, 3 × 3, and 1 × 1; the convolution kernel had a stride of 1. In addition, we introduced a shortcut connection into the convolutional layer.

Figure 2

Workflow of the SR-CNN Network. (a) Workflow of the Detection Model (b) Workflow of the Restoration Model. The whole framework first detects high-noise outliers via sliding region analysis, then repairs outliers to realize noise homogenization.



2.3.1.2 Sliding Region Generator

Since the detection target was the neighborhood of each point in the input image, the size was fixed. Therefore, we incorporated a region proposal generator, with a stride of approximately 1, and a fixed size of 3 × 3. The sliding region generator is designed to extract the local neighborhood of each pixel in the LDCT image. It slides over the entire image with a fixed 3×3 window and a stride of 1. Each sliding window corresponds to the local neighborhood of a single target pixel. Since outliers are defined as pixels with abnormal noise in local areas, extracting neighborhood features via the sliding window is a prerequisite for accurate outlier judgment. This mechanism ensures that the model always judges each pixel based on its surrounding contextual information, rather than relying on isolated pixel intensity.

2.3.1.3. Classifier

The classifier employs a binary classification model, mapping the generated candidate boxes onto the feature map for classification.

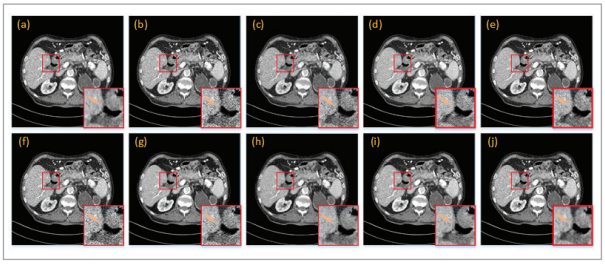
2.3.2. Image Inpainting Model

To achieve a uniform noise intensity distribution in LDCT images and ensure consistency with the input requirements of existing LDCT methods, we utilized an image inpainting approach. The outliers detected by the detection model were treated as missing points, and an image restoration model was employed to maintain a consistent noise intensity distribution in LDCT images. Since the missing regions in this study were outliers, only a shallow restoration network was required. Additionally, atrous convolution was used to expand the receptive field without increasing the number of network layers. The image restoration model adopts the basic architecture of a U-Net network, The image restoration module is based on the standard U-Net architecture. It simplifies the number of network layers and adds atrous convolution, as illustrated in Figure 2(b).

The complete end-to-end workflow of the proposed framework is described as follows. First, raw LDCT images are fed into the well-trained outlier detection model to identify pixels with excessive noise. Subsequently, the detected high-noise outliers are treated as missing regions and reconstructed via the image restoration module, which homogenizes the noise intensity across the entire LDCT image. Afterwards, the preprocessed images with uniform noise distribution are delivered to conventional denoising approaches, to implement the final denoising operation. Ultimately, the fully processed denoised LDCT images are generated as the final output.

Figure 3

Qualitative results of a 25% dose abdomen CT image from the Mayo 2016 dataset: (a) NDCT, (b) NLM, (c) Dn-Dp, (d) RED-CNN, (e) CTformer, (f) LDCT, (g) SR-CNN + NLM, (h) SR-CNN + Dn-Dp, (i) SR-CNN + RED-CNN, (j) SR-CNN + CTformer.



For image visualization and analysis, a viewing window with parameters of −160/240 HU was applied; additionally, the red-highlighted ROI was enlarged to facilitate visual comparison, and the target lesion was distinctly marked with an orange arrow. (g), (h), (i), and (j) represent using the output of the SR-CNN network as input for the NLM, Dn-Dp, RED-CNN, and CTformer methods, respectively. This figure proves that combining our SR-CNN preprocessing can significantly improve the visual effect of various mainstream denoising methods.

3. Results

3.1. Method Comparison

We retrained all models using publicly available code. We visually compared the denoising performance by using SR-CNN processed LDCT images as input compared to using LDCT images directly as input for these methods. The experimental results are shown in Figure 3(a)-(j); An orange arrow is used to indicate the lesion located within the red region of interest (ROI). Comparatively, the NLM algorithm had poorer denoising results, leaving noticeable noise artifacts. The Dn-Dp method, due to unsupervised learning, had slightly lower denoising performance than the RED-CNN method. The CTformer

method achieved better denoising results. However, using SR-CNN processed LDCT images as input for these methods yielded better denoising performance and texture closer to NDCT images than using LDCT images directly as input.

The above quantitative metrics and qualitative images verify the effectiveness of our method. The essential reason for the performance improvement is that SR-CNN eliminates spatially heterogeneous noise via preprocessing. After noise homogenization, the input characteristics of LDCT images match the design assumptions of most existing denoising models, which greatly reduces the denoising difficulty. The models no longer need to adapt to huge noise differences in different regions, thus achieving better PSNR, SSIM and other indicators. The proposed SR-CNN preprocess eliminates local high-noise outliers and unifies the noise intensity of the whole image. On this basis, subsequent denoising algorithms no longer need to adapt to strong noise differences in different regions. It reduces the difficulty and calculation burden of denoising models. Meanwhile, our method only targets high-noise abnormal points and retains the original structural information of low-noise areas, which effectively avoids the over-smoothing problem existing in traditional global denoising.

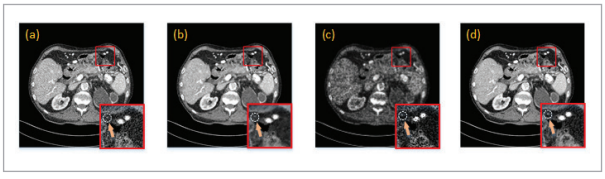
Table 1 Presents the quantitative results of various methods. We calculated the PSNR, SSIM, and RMSE for all images. The results indicate that using SR-CNN processed LDCT images as input for NLM, Dn-Dp, RED-CNN, and CTformer methods outperforms the original methods. On average, compared to the original methods, we achieved improvements of +1.5283 dB PSNR, +0.8% SSIM, and -4.9116 HU RMSE, consistent with visual assessments.

For image visualization and analysis, a viewing window with parameters of −160/240 HU was applied; additionally, the red-highlighted ROI was enlarged to facilitate visual comparison, and the target lesion was distinctly marked with an orange arrow. The results show that SR-CNN accurately removes high-noise outliers while effectively protecting fine image structures and lesion details.

Table 1
Quantitative Results (Mean) on 25% Dose Testing Data.

	PSNR (dB) ↑	SSIM↑	RMSE (HU)↓
LDCT	31.5608	0.8153	30.4161
NLM	35.6654	0.8316	27.5255
SRC+NLM	37.0360	0.8474	23.2465
Dn-Dp	37.2954	0.8538	22.2465
SRC+Dn-Dp	38.9759	0.8615	17.5134
RED-CNN	37.6513	0.8540	21.9668
SRC+RED-CNN	39.2133	0.8603	16.1340
CTformer	38.1599	0.8699	19.8858
SRC+CTformer	39.6602	0.8738	15.0843

Figure 4
Impact of SR-CNN Network on fine structures. (a) LDCT, (b) NDCT,(c) Outliers (black points represent outliers), (d) SR-CNN.



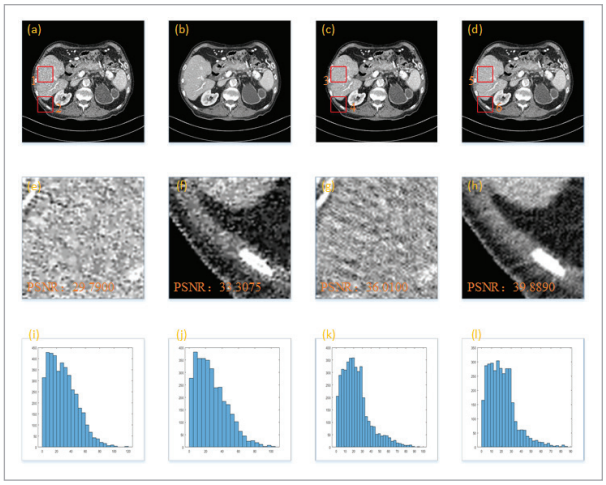
3.2. Impact of the SR-CNN Network on Fine Structures

To evaluate the impact of the SR-CNN network on fine structures, experimental results are shown in Figure 4(a)-(d); An orange arrow labels the location of the lesion within the red ROI. Despite detecting a considerable number of outliers, the introduction of structural similarity measures in outlier detection ensured that outliers were distributed more in flat regions and avoided concentrated distribution. As a result, the SR-CNN network effectively preserved fine structures.

3.3. Influence of Noise Intensity Distribution

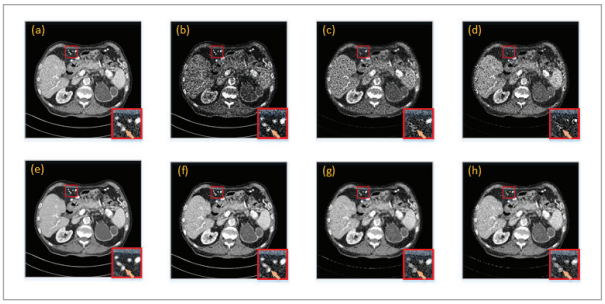
Generally speaking, the noise intensity distribution in LDCT images is not uniform. In order to verify the influence of noise intensity distribution, the LDCT image is evenly divided into 64 small blocks, where the LDCT image comes from slices of low-dose (quarter) CT images with a thickness of 3.0 mm in 2016 NIH-AAPM Mayo Clinic LDCT Grand Challenge dataset. The size of the LDCT image is

Figure 5
Influence of noise intensity distribution. (a) LDCT, (b) NDCT (c) SR-CNN, (d) RED-CNN, (e) The red ROI 1 Zoom in image, (f) The red ROI 2 Zoom in image, (g) The red ROI 5 Zoom in image, (h) The red ROI 6 Zoom in image, (i) Noise intensity distribution in red ROI 1, (j) Noise intensity distribution in red ROI 2, (k) Noise intensity distribution in red ROI 3, (l) Noise intensity distribution in red ROI 4. The display window is [-160, 240] HU. This figure demonstrates that SR-CNN can significantly homogenize the noise intensity of different local regions.



512×512, and the size of each small block is 64×64. The PSNR index is selected as the basis for judging the noise intensity. The smaller the PSNR value, the higher the noise intensity. The experimental results are shown in Figure 5(a)-(l). From 64 small blocks of LDCT image segmentation, the minimum value of PSNR index is selected as the red ROI 1, and the maximum value of PSNR index is selected as the red ROI 2. Select the same region in the SR-CNN result diagram as the red ROI 3 and the red ROI 4. Select the corresponding regions in the RED-CNN result diagram that match the locations of red ROI 5 and red ROI 6. By comparing red ROI 1 with red ROI 5, it is evident that the RED-CNN method exhibits limited denoising effectiveness in areas characterized by high noise intensity. In contrast, when comparing red ROI 2 with red ROI 6, the RED-CNN method demonstrates superior denoising performance in regions with lower noise intensity. Furthermore, the comparison between red ROI 5 and red ROI 6 reveals that the denoising capability of the RED-CNN method varies depending on the noise intensity within

Figure 6
Comparison of different anomaly detection methods. (a) LDCT image, (b) outliers detected by SR-CNN (black dots denote outliers), (c) outliers detected by the Z-score method (black dots denote outliers), (d) outliers detected by principal component analysis (black dots denote outliers), (e) NDCT image, (f) restoration result of the proposed method, (g) restoration result of the Z-score method, (h) restoration result of PCA. The display window is set to −160 to 240 HU. The red ROI is magnified for visual comparison, and the orange arrow indicates a tiny bony region.



different regions of the same image. Figures 5(i)-(l) illustrate the noise intensity distribution across red ROIs 1-4. where the horizontal axis represents noise intensity, and the vertical axis represents the number of pixels corresponding to the noise intensity. The results of Figures 5(i)-(l) show that the SR-CNN method can make the noise intensity distribution in different regions of LDCT image more uniform, and make the noise intensity concentrate on low noise intensity, so as to effectively improve the denoising performance of the denoising algorithm.

3.4. Ablation Study

In this subsection, we perform an ablation study to thoroughly evaluate the contribution of each component in the proposed method, with a particular focus on the detection module. To validate its effectiveness, we compare it with classical traditional detection methods, including the Z score thresholding method and principal component analysis (PCA).

As shown in Figure 6(a)-(h), both the Z score thresholding and PCA misclassify subtle anatomical details as anomalous regions, resulting in the loss of fine structural information in the final processed images—for example, the tiny bony regions indicated by the arrows in Figure 6.

This is because the Z score thresholding method relies solely on pixel level intensity statistics. For subtle details, which exhibit abrupt intensity variations, valid anatomical information is easily misidentified as outliers. PCA, by contrast, extracts low dimensional principal features based on intensity correlations and detects anomalies according to reconstruction error. However, subtle details correspond to high frequency information that cannot be adequately captured by a small set of principal components. Consequently, such details tend to be discarded during dimensionality reduction and reconstruction, which significantly increases the reconstruction error and leads to false detection. In comparison, the detection module of the proposed SR CNN incorporates structural similarity weights and other constraints, enabling it to effectively preserve subtle anatomical details.

4. Discussion

4.1. Key Contributions and Mechanism Analysis

In the field of low-dose CT (LDCT) image denoising, factors such as tube current, CT positioning, and slice thickness result in an uneven noise intensity distribution in LDCT images. Most traditional LDCT methods treat LDCT images as a whole and do not feature specific modules to handle varying noise intensities, leading to overly uniform denoising capabilities. Low noise intensities may result in excessive smoothing, while high noise intensities may result in insufficient denoising. Additionally, although different LDCT methods employ various denoising strategies, the denoising performance of these strategies cannot be combined. This is because these methods, despite their denoising capabilities, do not change the inherent uneven noise intensity distribution of LDCT images. In fact, the results after denoising may exacerbate this uneven distribution. On the other hand, newer LDCT methods with stronger denoising performance produce outputs with noise intensity distributions more concentrated in low-noise regions. When used as input for other methods, this leads to a weaker overall denoising capability and subsequently degrades the overall denoising performance. Addressing the uneven noise intensity distribution in LDCT images can further exploit the denoising potential of existing LDCT methods. In this paper, we propose the SR-CNN method, a general preprocessing approach based on outlier detection to address the uneven noise intensity distribution in LDCT images.

In this study, we analyzed the noise intensity distribution in LDCT images and found that low-noise-intensity pixels account for the majority of the total pixel count, while high-noise-intensity pixels comprise only a small fraction. Based on this, we defined points with higher noise intensity as outliers and designed an outlier detection network using a detection model to identify these outliers in LDCT images. Subsequently, we used image inpainting techniques to treat the detected outliers as missing points, restoring the LDCT images to a uniform noise intensity distribution consistent with the inputs required by existing LDCT methods. After cascading our SR-CNN preprocessing module, every mainstream denoising baseline achieves better quantitative metrics than running the model alone. Such consistent performance improvement comes from the synergistic design of structural-aware outlier detection and image restoration submodules. Firstly, we addressed the uneven noise intensity distribution in LDCT images, further leveraging the denoising capabilities of existing LDCT methods without necessitating redesigns. This is a novel aspect not covered by other methods. Secondly, we introduced similarity measures during outlier detection, preventing the loss of structural information.

Most existing denoising models are designed for overall uniform noise. When facing LDCT with heterogeneous noise, their denoising ability is limited. Our preprocessing module homogenizes noise in advance, which matches the applicable scenarios of mainstream denoising algorithms, thereby fully activating their inherent denoising potential. In addition, combined with structural similarity constraints in outlier detection, our method can protect edge and tissue details while removing strong noise, which is another key reason for the improvement of SSIM and visual quality.

4.2. Practical Clinical and Engineering Implications

Our study demonstrates the efficacy of the outlier detection based denoising algorithm in significantly reducing noise artifacts and enhancing image quality in LDCT scans. By integrating traditional and deep learning approaches, we achieved notable

improvements in image clarity and detail preservation. These findings hold significant implications for clinical practice, particularly in the field of diagnostic imaging. An enhancement in the quality of LDCT images can lead to more accurate and reliable diagnoses, thus enabling healthcare providers to make better-informed treatment decisions. Moreover, a reduction in noise artifacts may improve patient comfort during imaging procedures and reduce the need for repeated scans, ultimately enhancing the overall efficiency of healthcare.

4.3. Inherent Limitations and Future Work

However, our algorithm still has some limitations. First, the proposed method is a preprocessing module and does not replace end-to-end denoising models; its performance gain depends on the baseline denoising method. Second, the restoration module treats outliers as missing pixels, which is a simple strategy and may not fully recover complex tissue textures. Third, all experiments are conducted on the Mayo 2016 abdominal LDCT dataset (25% dose, 3.0 mm slice thickness); generalization to other body regions, dose levels, or scanners requires further validation. Fourth, the detection model relies on supervised training with LDCT-NDCT pairs, which may limit its applicability in scenarios with limited paired data.

Despite these limitations, SR-CNN offers a practical and effective preprocessing solution for LDCT denoising. Future work will focus on developing more advanced outlier detection and restoration modules, validating the method on multi-center and multi-scanner datasets, and extending the framework to other medical imaging modalities.

5. Conclusion

In summary, we proposed a novel general preprocessing method to address the uneven noise intensity distribution in LDCT images. Qualitative and quantitative results on the 2016 NIH-AAPM Mayo Clinic LDCT Grand Challenge dataset show that our method outperforms both directly using LDCT images as input and using the outputs of other LDCT methods as input. However, challenges remain, and we are committed to further overcoming these obstacles.

Declaration of Conflicting Interests

The author(s) declared no potential conflicts of interest with respect to the research, author-ship, and/or publication of this article.

Data Sharing Agreement

The datasets used and/or analyzed during the current study are available from the corresponding author on reasonable request.

Funding

The author(s) received no financial support for the research, authorship, and/or publication of this article.

References

1. Bera, S., Biswas, P. K. Noise-Conscious Training of Non-Local Neural Network Powered by Self-Attentive Spectral-Normalized Markovian Patch GAN for Low-Dose CT Denoising. IEEE Transactions on Medical Imaging, 2021, 40(12), 3663-3673. https://doi.org/10.1109/TMI.2021.3094525
2. Chefer, H., Gur, S., Wolf, L. Transformer Interpretability Beyond Attention Visualization. Proceedings of the IEEE/CVF Conference on Computer Vision and Pattern Recognition, 2021, 782-791. https://doi.org/10.1109/CVPR46437.2021.00084
3. Chen, H., Zhang, Y., Kalra, M. K., Lin, F., Chen, Y., Liao, P., Zhou, J., Wang, G. Low-Dose CT with a Residual Encoder-Decoder Convolutional Neural Network. IEEE Transactions on Medical Imaging, 2017, 36(12), 2524-2535. https://doi.org/10.1109/TMI.2017.2715284
4. Di Feola, F., Tronchin, L., Guarrasi, V., Soda, P. Multi-Scale Texture Loss for CT Denoising with GANs. AI Open, 2025. https://doi.org/10.1016/j.aiopen.2025.09.001
5. Diwakar, M., Kumar, M. A Review on CT Image Noise and Its Denoising. Biomedical Signal Processing and Control, 2018, 42, 73-88. https://doi.org/10.1016/j.bspc.2018.01.010
6. Gao, Q., Hongming, S. CoCoDiff: A Contextual Conditional Diffusion Model for Low-Dose CT Image De-

noising. Developments in X-Ray Tomography XIV, 2022, 12242. https://doi.org/10.1117/12.2634939

7. Gao, Q., Li, Z., Zhang, J., Zhang, Y., Shan, H. CoreDiff: Contextual Error-Modulated Generalized Diffusion Model for Low-Dose CT Denoising and Generalization. IEEE Transactions on Medical Imaging, 2024, 43(2), 745-759. https://doi.org/10.1109/TMI.2023.3320812
8. Han, M., Baek, J. Low-Dose CT Denoising via CNN Trained Using Images with Activation Map. Medical Imaging: Image Perception, Observer Performance, and Technology Assessment, 2022, 12035. https://doi.org/10.1117/12.2607720
9. Hojjat, M., Shayegan, M. J., Ghadami, O. Low-Dose CT Image Denoising Based on EfficientNetV2 and Wasserstein GAN. 2024 10th International Conference on Web Research (ICWR), 2024, 195-201. https://doi.org/10.1109/ICWR61162.2024.10533377
10. Huang, Z., Zhang, J., Zhang, Y., Shan, H. DU-GAN: Generative Adversarial Networks with Dual-Domain U-Net-Based Discriminators for Low-Dose CT Denoising. IEEE Transactions on Instrumentation and Measurement, 2022, 71, 1-12. https://doi.org/10.1109/TIM.2021.3128703
11. Jin, H., Tang, Y., Liao, F., Du, Q., Wu, Z., Li, M., Zheng, J. Adaptive Noise-Aware Denoising Network: Effective Denoising for CT Images with Varying Noise Intensity. Biomedical Signal Processing and Control, 2024, 96, 106548. https://doi.org/10.1016/j.bspc.2024.106548
12. Junhua, C., Leonard, W., Andre, D., Inigo, B. Improving Reproducibility and Performance of Radiomics in Low-Dose CT Using Cycle GANs. Journal of Applied Clinical Medical Physics, 2022, 23(10). https://doi.org/10.1002/acm2.13739
13. Kawar, B., Elad, M., Ermon, S., Song, J. Denoising Diffusion Restoration Models. Advances in Neural Information Processing Systems, 2022. https://doi.org/10.52202/068431-1714
14. Kim, B., Han, M., Shim, H., Baek, J. A Performance Comparison of Convolutional Neural Network-Based Image Denoising Methods: The Effect of Loss Functions on Low-Dose CT Images. Medical Physics, 2019, 46, 3906-3923. https://doi.org/10.1002/mp.13713
15. Le Quoc, A., Loc, P. X., Ha, L. M. Impact of Image Denoising Techniques on CNN-Based Liver Vessel Segmentation Using Synthesis Low-Dose Contrast-Enhanced CT Images. Electronics & Communications, 2023, 12(3-4). https://doi.org/10.21553/rev-jec.315
16. Li, H., Yang, X., Yang, S., Wang, D., Jeon, G. Transformer with Double Enhancement for Low-Dose CT Denoising. IEEE Journal of Biomedical and Health Informatics, 2022. https://doi.org/10.1109/JBHI.2022.3216887
17. Li, R. Diffusion Denoising for Low-Dose CT Model. arXiv, 2023. Available at: https://arxiv.org/abs/2301.11482
18. Li, Z., Liu, Y., Chen, Y., Shu, H., Lu, J., Gui, Z. Dual-Domain Fusion Deep Convolutional Neural Network for Low-Dose CT Denoising. Journal of X-Ray Science and Technology, 2023, 31(4), 757-775. https://doi.org/10.3233/XST-230020
19. Liu, X., Xie, Y., Liu, C., Cheng, J., Diao, S., Tan, S., Liang, X. Diffusion Probabilistic Priors for Zero-Shot Low-Dose CT Image Denoising. Medical Physics, 2025, 52(1), 329-345. https://doi.org/10.1002/mp.17431
20. Nagare, M., Melnyk, R., Rahman, O., Sauer, K. D., Bouman, C. A. A Bias-Reducing Loss Function for CT Image Denoising. Proceedings of the IEEE International Conference on Acoustics, Speech and Signal Processing, 2021, 1175-1179. https://doi.org/10.1109/ICASSP39728.2021.9413855
21. Scetbon, M., Elad, M., Milanfar, P. Deep K-SVD Denoising. IEEE Transactions on Image Processing, 2021, 30, 5944-5955. https://doi.org/10.1109/TIP.2021.3090531
22. Smith-Bindman, R., Lipson, J., Marcus, R., Kim, K. P., Mahesh, M., Gould, R. Radiation Dose Associated with Common Computed Tomography Examinations and the Associated Lifetime Attributable Risk of Cancer. Archives of Internal Medicine, 2009, 169, 2078-2086. https://doi.org/10.1001/archinternmed.2009.427
23. Sodickson, A., Baeyens, P. F., Andriole, K. P., Prevedello, L. M., Nawfel, R. D., Hanson, R., Khorasani, R. Recurrent CT, Cumulative Radiation Exposure, and Associated Radiation-Induced Cancer Risks from CT of Adults. Radiology, 2009, 251, 175-184. https://doi.org/10.1148/radiol.2511081296
24. Song, Y., Shen, L., Xing, L., Ermon, S. Solving Inverse Problems in Medical Imaging with Score-Based Generative Models. International Conference on Learning Representations, 2022.
25. Song, Y., Sohl-Dickstein, J., Kingma, D. P., Kumar, A., Ermon, S., Poole, B. Score-Based Generative Modeling Through Stochastic Differential Equations. International Conference on Learning Representations, 2021. https://doi.org/10.52202/075280-1645
26. Wang, D., Fan, F., Wu, Z., Liu, R., Wang, F., Yu, H. CTformer: Convolution-Free Token2Token Dilated Vi-

sion Transformer for Low-Dose CT Denoising. Physics in Medicine & Biology, 2023, 68(6), 065012. https://doi.org/10.1088/1361-6560/acc000

27. Wu, C., Gao, T. Application of BM3D Algorithm in CT Image Denoising of Liver Cancer. Proceedings of the 2nd International Conference on Computer Vision, Image, and Deep Learning, 2021, 11911, 388-398. https://doi.org/10.1117/12.2604518
28. Xia, W., Shi, Y., Niu, C., Cong, W., Wang, G. Diffusion Prior Regularized Iterative Reconstruction for Low-Dose CT. arXiv, 2023. DOI: https://doi.org/10.48550/arXiv.2310.06949
29. Xiao, Z., Kreis, K., Vahdat, A. Tackling the Generative Learning Trilemma with Denoising Diffusion GANs. International Conference on Learning Representations, 2022. Available at: https://arxiv.org/abs/2112.07804
30. Yang, L., Zhang, Z., Song, Y., Hong, S., Xu, R., Zhao, Y., Zhang, W., Cui, B., Yang, M. H. Diffusion Models: A Comprehensive Survey of Methods and Applications. ACM Computing Surveys, 2024, 56(4), 1-39. https://doi.org/10.1145/3626235
31. Yin, Z., Zheng, Z. Segmentation as Domain Knowledge in GAN for Low-Dose CT Denoising. Journal of Imaging Science and Technology, 2022, 66(4), 040415-1-040415-7. https://doi.org/10.2352/J.ImagingSci.Technol.2022.66.4.040415
32. Yuan, J., Zhou, F., Guo, Z., Li, X., Yu, H. HCformer: Hybrid CNN-Transformer for LDCT Image Denoising. Journal of Digital Imaging, 2023, 36(5), 2290-2305. https://doi.org/10.1007/s10278-023-00842-9
33. Yuan, L., Chen, Y., Wang, T., Yu, W., Shi, Y., Jiang, Z. H., Tay, F. E., Feng, J., Yan, S. Tokens-to-Token ViT: Training Vision Transformers from Scratch on ImageNet. Proceedings of the IEEE/CVF International Conference on Computer Vision, 2021, 558-567. https://doi.org/10.1109/ICCV48922.2021.00060
34. Zhang, J., Zhou, H., Niu, Y., Lv, J., Chen, J., Cheng, Y. CNN and Multi-Feature Extraction Based Denoising of CT Images. Biomedical Signal Processing and Control, 2021, 67, 102545. https://doi.org/10.1016/j.bspc.2021.102545
35. Zhang, Z., Yu, L., Liang, X., Zhao, W., Xing, L. TransCT: Dual-Path Transformer for Low-Dose Computed Tomography. International Conference on Medical Image Computing and Computer-Assisted Intervention, 2021, 12903, 58-68. https://doi.org/10.1007/978-3-030-87231-1_6
36. Zhao, C., Wu, S., Wu, J. Parameter-Adaptive NLM Denoising Algorithm Based on Hessian Matrix. 2021 4th International Conference on Intelligent Autonomous Systems (ICoIAS), 2021, 216-221. https://doi.org/10.1109/ICoIAS53694.2021.00046

This article is an Open Access article distributed under the terms and conditions of the Creative Commons Attribution 4.0 (CC BY 4.0) License (http://creativecommons.org/licenses/by/4.0/).